ISSN 1023-1935, Russian Journal of Electrochemistry, 2014, Vol. 50, No. 12, pp. 1118–1126. © Pleiades Publishing, Ltd., 2014.
Original Russian Text © S.V. Shevkunov, 2014, published in Elektrokhimiya, 2014, Vol. 50, No. 12, pp. 1250–1259.

The Hydrate Shell of a Cl^- Ion in a Planar Nanopore, Structure

S. V. Shevkunov[z]

Saint Petersburg State Polytechnical University, Politekhnicheskaya 29, St. Petersburg, 195251 Russia

Received October 18, 2013

Abstract—The formation of nanoelectrolyte is simulated by the Monte-Carlo method in the stage of penetration of solvent molecules into a nanopore that contains one ion. The detailed model of many-body intermolecular interactions including covalent interactions and the effects of bond saturation and excessive charge transfer is used. The molecular structure of the chloride-anion hydrate shell growing from water vapors at 298 K inside planar model pores with smooth walls and the width of 0.5 and 0.7 nm is analyzed. The maxima of the space correlation function ion–molecule are not shifted in the pore. The pore induces changes mainly in the orientational molecular order of the system. The effect of molecules that "creep" over the pore surface in the ion field is revealed. The earlier observed effect of ion displacement from its hydrate shell to the periphery of the molecular cluster is reproduced stably.

Keywords: nanoelectrolyte, planar nanopore, molecular structure, hydrate shell, chloride anion

DOI: 10.1134/S1023193514120088

INTRODUCTION

The mechanism of hydration of charges at surfaces is the key problem in theoretical investigation of the wide range of phenomena from electrochemical reactions on electrodes in aqueous electrolytes, metal corrosion, and chemical catalysis to the heterogeneous nucleation of atmospheric moisture on the surface of crystalline aerosol. Porous electrodes are used in electrochemical systems for enhancing the capacity of accumulating cells with respect to ions and electrons, intensifying the charge transfer, and accelerating the reactions occurring on the surface [1–3]. If a gaseous medium, a liquid electrolyte, and a solid catalyst must be brought simultaneous into contact, as in the majority of fuel cells and storage batteries, then this problem can be solved only with the use of porous structures.

The behavior of electrolytes in nanopores on the surface of porous electrodes qualitatively differs from that in bulk solutions. The porosity can considerably increase the effective surface of the material and its susceptibility towards electrosorption. The interest in synthesizing materials with high electrosorptive parameters is due to their numerous applications including the technology of water purifying [4–6].

The transition layer at the contact with the pore walls can occupy the larger part of the pore volume so that all electrolyte in the nanopore pertains completely to the transition layer. If the crystalline surface layer of the wall carries an electric charge, the dissolved ions form the electric double layer at it with the thickness varying from one to several nm [7, 8]. Depending on the pore width, this layer can overlap the analogous layer formed at the opposite wall. As a result, there arises a strong dependence of electrolyte properties on geometrical dimensions of pores and the porous structure as a whole.

In the first approximation, the structure of electrolyte that fills the pore can be assessed in terms of the classical theory of Gouy–Chapman [9–11] based on the mean field approximation and stemming from the Poisson–Boltzmann equation for the spatial distribution of charges; however, this approximation is true only in the limit of strongly dilute electrolytes. At the same time, in dilute electrolytes the Debye radius can exceed the pore width, making this approach wrong for nanopores.

The more thorough methods which are based on integral equations and, in particular, the hyperchain approximation [10, 11] contain a number of approximations stemming from the condition of closure of the chain of integro-differential equations and also assuming the presence of the substantial, albeit weaker, dilution and relatively weak inter-ion correlations.

The methods of computer simulation are free of these limitations. In the pioneering studies [12–16], the Monte-Carlo method was used for investigation of the equilibrium properties of the electric double layer formed in planar nanopores filled with aqueous electrolyte with univalent ions. In the later studies [17–26], it was found that asymmetrical electrolytes with polyvalent ions can behave quite peculiarly in pores. Particularly, it was shown that smaller ions approach the wall surface with the higher probability. In asymmetrical electrolytes, in the double layer, the charge inversion effect is possible. Later [27], the Monte-Carlo method

[z] Corresponding author: shevk54@mail.ru (S.V. Shevkunov).

was used for studying the effects of asymmetry in a slit pore. The crystal structure of walls and the molecular structure of the solvent were not taken into account explicitly. A mixture of trivalent and univalent ions of the opposite sign was simulated. It was found that in the pore central part 2 nm wide, the local charge density of oppositely charged ions was not leveled off in solutions with low concentration. The combination of asymmetry with respect to charge and asymmetry with respect to ion size leads to differently directed effects in the charge density distribution and electric double layer configurations. The coarser ions are forced out into the inner part of the pore, whereas the charge larger in the absolute value favors drawing the ion to the walls. Under conditions of the high charge density on pore walls, the distributions of the local density of ions at the walls cease to be monotonic and become oscillating. Near the wall, a layer can form in which the charges with the same sign as on the wall predominate.

Although the model studied in [27] is severely simplified, it provides guidelines over the diversity of phenomena in nanoelectrolytes and demonstrates sensitivity of size effects with respect to the ratio of charge and size of counter ions. It is acknowledged that due to the smallness of this system, the electroneutrality condition can be violated in nanopores even if only one ion is present in an electrolyte-filled pore [28, 29].

The theoretical studies of electrolytes in pores accomplished so far considered the conditions of a pore in contact with a bulk liquid electrolyte and completely filled with the latter. The conditions of a pore in contact with water vapors, which allow partial filling of the pore, were not considered. At the same time, these conditions are of interest not only in connection with phenomena observed on surfaces in contact with the natural atmosphere but also in bulk electrolytes when the electrochemical process on the electrode surface is accompanied by evolution of gaseous components.

Nanosized cavities such as fractures and cracks can provide conditions for hydrated ions substantially different from the bulk vapor conditions. The hydration in a small volume depends largely on two factors: the severe steric limitations for the ion and the direct interactions of the hydrate shell with pore walls. It is reasonable to try to separate the contributions of these factors, although their complete separation is of course impossible. At the same time, whereas the relationships associated with spatial limitations can be relatively universal, the effects caused by interactions with the walls are determined by the particular crystalline structure of the surface and depend cardinally on the nature of the particular material.

In this study, we consider the effect of the limited volume of the system on the formation of the hydrate shell of a single-charged chloride anion. To separate the effects of the limited volume from the consequences caused by details of molecule interaction with the cavity walls, the structure-free solid wall are simulated.

2. SIMULATION CONDITIONS

The model pore represents the space between two parallel planes located at a fixed distance. The numerical calculations were accomplished for two values of pore width: 0.5 and 0.7 nm. The first value was chosen in order to have a pore with the width commensurate with the diameter of the first hydrate layer and also to provide sufficiently pronounced effects of perturbations in the hydrate shell structure. The second value was taken in order to assess how under these conditions the structure and thermodynamic characteristics of the ion hydrate shell depend on the pore width. Inside the pore, the molecules move freely, interacting with the other molecules and ions. The ion is fixed in the center between the pore walls.

In the pore plane, no periodic boundary conditions were implied on the system, because the system with the only ion is not electroneutral. The presence of the infinite number of periodically repeated images of the ion would mean the violation of the principle of system electroneutrality on the macroscopic scale. In the explicit form, we simulated the microscopic part of the totally electroneutral system. The microscopic volume accessible for the molecular motion represents the superposition of the space between pore walls and the interior of the sphere with 2-nm radius circumscribed around the ion center. Numerical calculations were carried out for systems involving up to 100 water molecules. The molecules find themselves drawn into the ion field and form naturally its hydrate shell with spatial dimensions much smaller than the mentioned radius of the limiting sphere. Hence, the limiting sphere introduces no substantial perturbations into the shell structure but its presence is necessary in order to separate the region of explicit description from the thermostat region the material contact with which is described by the Gibbs statistical methods.

We simulated the successive growth of the hydrate shell by adding one molecule each time. After being introduced into the microvolume, the molecule could freely move in the field of other molecules and the ion according to the function of distribution of the canonical statistical assembly [30]. For this purpose, by means of a computer, the steps of spatial shifts and turns of all molecules were simulated with standard probabilities of the Monte Carlo method [31], by using the random number generator. The thermalization of the system took 5×10^7 steps. The calculation of equilibrium averages was accomplished by direct averaging over the series of 10^8 configurations. The frequency of formation of new configurations varied in the range from 30 to 50% at the maximum translational shift of a molecule by 0.03 nm and the maximum rotation angle of 20°.

The input parameters of statistical mechanical simulations are intermolecular interactions expressed as intermolecular potentials. As a rule, statistical-mechanical simulation of electrolytes and hydrated

ions involves the use of the simplest pair model potentials in which the interaction of water molecules with ions are described in the form of Coulomb terms in combination with the Lennard-Jones potential which represents the dispersion and exchange forces. The pair models of electrolytes assume that the energy of the system as a whole represents a sum of individual pair interactions of molecules between one another and with ions [32–38].

In electrolyte models that claim the explicit consideration of polarization interactions, the polarization energy of molecules in the ion field which usually represents the first term of multipole series is added to the pair interactions [39–44]. However, the multipole expansion represents a series over powers of reciprocal distance to the electric field source which converges only at sufficiently long distances exceeding the space dimensions of the source, i.e., the molecular size. At such distances, the polarization energy at room temperature T is far smaller than the characteristic average kinetic energy of thermal motion k_BT and hence can substantially affect the statistical behavior of the system only due to addition of fields of numeral individual molecules in the vicinity of the polarizing charge. However, this collective effect also turns out to be considerably weakened due to the relatively fast ($\propto r^{-4}$) decrease in the polarization energy with the distance. At the same time, the polarization interactions at distances comparable with the size of average molecules cannot be described by only the first term of the multifield series.

In [45–47], an attempt was undertaken to solve this problem by representing the molecular field as a field of a complex system of point charges and polarized point centers fixed in the body of a molecule or an ion (the method of distributed polarizability). The optimal distribution of several tens or several hundreds of such centers is supposed to be selected by the iteration method in order to reproduce the interaction of particles for a certain set of their mutual orientations with the maximum accuracy. Moreover, it is assumed that quantum-mechanical effects caused by the exchange and the partial collectivization of electron orbitals can be successfully approximated by a combination of elementary electrostatic interactions. Such an assumption seems to be open to question. Particularly, strong many-body interactions, the extreme manifestation of which is the effect of saturation of chemical bonds and the valence, can hardly be represented as the simplest electrostatic interactions in a system of rigidly fixed charges and polarization centers.

In [48–51], we decided to reject the purely electrostatic model and developed a detailed many-body model of interactions of ions with water molecules ICP(SPC) (Ions + Covalent bonds + Polarization (based on the SPC geometry)) which, in addition to the Coulomb, exchange, polarization, and dispersion interactions, considers the polarization interactions in the form different from the first term in multipole expansions and also the strong many-body interactions of the covalent type, the energy of dipoles induced on molecules in the molecular field, the interaction of induced dipoles, and the effect of partial charge transfer which, in essence, is the limiting manifestation of the effect of polarization at contact distances between interacting particles. The numerical parameters of interactions were determined from the condition of the maximally accurate reproduction of experimental values of free energy and entropy of the reactions of attachment of vapor molecules to the hydrate shell of the ion.

In [52], the comparative statistical-mechanical calculations of free energy, entropy, and work on hydration of a Cl^- ion were performed numerically in terms of the traditional pair and the detailed many-body ICP(SPC) models. It was shown that in terms of the pair model, the curve of the free energy of attachment reactions demonstrates the substantially overrated slope, and the difference of the found values from the experimental ones is ca. $2k_BT$. As a result, the error was nearly one order of magnitude for the reaction rate of monomer attachment and 8 orders of magnitude for the rate of hydrate shell formation of a size in the range of 10–15 molecules. In the saturated vapor region, the equilibrium size of the hydrate shell and its growth rate with the increase in the vapor pressure are much overrated in the pair model. The experimental data and the detailed model of interactions give the value of 8 molecules for the stable size of the ion hydrate shell in saturated vapor at room temperature, whereas the pair model gives 25 molecules; moreover, this gap rapidly increases in the region of oversaturation. The oversized hydrate shell and its lower resistance with respect to the random growth in the pair model radically narrow down the region of metastable states in oversaturated vapors. In [53], the comparative statistical-mechanical calculations of the Na^+ ion hydrate shell structure in the primitive pair and many-body ICP(SPC) models were carried out. It was shown that the absence of interactions of induced dipoles in the primitive model leads to overestimation of the first coordination number in aqueous electrolytes by approximately unity.

In the present study, we use the IPS(SPC) model of interactions with the chloride ion. In this model, as applied to the case of a single ion in the system, the paired part of the water–water interaction $U_{\text{pair}}^{\text{W–W}}$ is described by the multi-centered potential SPC [54] with three point charges q_k:

$$U_{\text{pair}}^{\text{W–W}} = \sum_{i<j}\left\{4\varepsilon_0^{\text{W}}\left(\left[\frac{\sigma^{\text{W}}}{r_{ij}}\right]^{12} - \left[\frac{\sigma^{\text{W}}}{r_{ij}}\right]^{6}\right) + \sum_{k=0}^{2}\sum_{l=0}^{2}\frac{q_k q_l}{\left|\mathbf{r}_k^i - \mathbf{r}_l^j\right|}\right\}, \quad (1)$$

where $r_{ij} = |\mathbf{r}_{ij}|$, and $\mathbf{r}_{ij} = \mathbf{r}_0^j - \mathbf{r}_0^i$ is a vector connecting the centers of the ith and the jth molecules; $\mathbf{r}_k^i$ is the coordinate of the kth charge of the ith molecule. One of charges is located in the Lennard-Jones center ($\mathbf{r}_0^i$) and approximately corresponds to the position of the oxygen atom, while the other two charges in points $\mathbf{r}_1^i$ and $\mathbf{r}_2^i$ are rigidly fixed at the distance of 0.1 nm from oxygen on the rays that form the angle of 109.47° and approximately correspond to the position of hydrogen atoms in the molecule. From here on, for short, the Coulomb coefficient $1/4\pi\varepsilon_0$ is omitted from electrostatic formulas, i.e., the latter are represented in the form corresponding to the CGS system.

The electrostatic interaction of water molecules with the ion $U_{\text{coul}}^{\text{I(–)–W}}$ is written as a sum of Coulomb interactions between three point charges of molecules q_k^-, $k = 0, 1, 2$ and two point charges of the ion: screened at small distances Q_0^- and unscreened Q_1^-, which are located in the ion center in point $\mathbf{x}_0^-$:

$$U_{\text{coul}}^{\text{I(–)–W}} = \sum_i \left[\sum_{k=0}^{k=2} \frac{s_-(|\mathbf{r}_k^i - \mathbf{x}_0^-|)Q_0^- + Q_1^-}{|\mathbf{r}_k^i - \mathbf{x}_0^-|} q_k^- \right]. \quad (2)$$

The screening function of charge Q_0^-

$$s_-(R) = \begin{cases} 0 & 0 < R < R_L^- \\ (R - R_L^-)^2 (3R_U^- - R_L^- - 2R) / (R_U^- - R_L^-)^3 & R_L^- \le R \le R_U^- \\ 1 & R_U^- < R < \infty \end{cases}, \quad (3)$$

with characteristic radii R_l^- and R_U^- has the same form as the attenuation function of Rahman and Stilliger in ST2 potential [55].

The polarization energy of molecules in the field of ions is written as the first term of the multifield series

$$U_{\text{pol}}^{\text{I–W}} = -\frac{1}{2}\alpha_{\text{w}} \sum_i (\mathbf{E}^-(\mathbf{r}_0^i))^2, \quad (4)$$

where α_{w} is the isotropic part of the tensor of water molecule polarizability. The strength of the ion electric field consists of the field of screened and unscreened charges and is assessed by the formula

$$\mathbf{E}^-(\mathbf{r}) = \frac{[s_-(|\mathbf{r} - \mathbf{x}_0^-|)]^2 Q_0^-}{|\mathbf{r} - \mathbf{x}_0^-|^3} (\mathbf{r} - \mathbf{x}_0^-) + \frac{Q_1^-}{|\mathbf{r} - \mathbf{x}_0^-|^3} (\mathbf{r} - \mathbf{x}_0^-). \quad (5)$$

The energy of dipoles induced on molecules in the electric field of molecules

$$U_{\text{ind,perm}}^{\text{W–W}} = -\sum_j \mathbf{E}^{\text{W}}(\mathbf{r}_0^j)\mathbf{p}_j^{\text{ind}}. \quad (6)$$

The field of molecules in point $\mathbf{r}_0^j$ where the jth molecule is located

$$\mathbf{E}^{\text{W}}(\mathbf{r}_0^j) = \sum_{i \ne j} \sum_{k=0}^{2} \frac{q_k}{|\mathbf{r}_0^j - \mathbf{r}_k^i|^3} (\mathbf{r}_0^j - \mathbf{r}_k^i). \quad (7)$$

The dipole moment of the jth molecule induced by the field of ions $\mathbf{p}_j^{\text{ind}} = \alpha_{\text{w}} \sum_n \mathbf{E}^-(\mathbf{r}_0^j)$. The polarization energy of a ion with polarizability α_- in the field of molecules

$$U_{\text{pol}}^{\text{I}(n)–(\text{WI})} = -\frac{\alpha_-}{2}(\mathbf{E}_{\text{I}}^{\text{W}}(\mathbf{x}_0^-))^2 = -\frac{\alpha_-}{2}\left(\sum_i \sum_{k=0}^{2} \frac{q_k^-}{|\mathbf{x}_0^- - \mathbf{r}_k^i|^3} (\mathbf{x}_0^- - \mathbf{r}_k^i) \right)^2. \quad (8)$$

The energy of interaction of dipoles induced on molecules

$$U_{\text{ind,ind}}^{\text{W–W}} = \sum_{i<j} \left[\frac{(\mathbf{p}_i^{\text{ind}} \mathbf{p}_j^{\text{ind}})}{(r_{ij})^3} - 3\frac{(\mathbf{p}_i^{\text{ind}} \mathbf{r}_{ij})(\mathbf{p}_j^{\text{ind}} \mathbf{r}_{ij})}{(r_{ij})^5} \right]. \quad (9)$$

The exchange and dispersion interaction between the ion and the molecules are set as the Lennard-Jones potential

$$U_{\text{LD}}^{\text{I–W}} = \sum_i 4\varepsilon_0^- \left(\left[\frac{\sigma_-}{R_{-i}} \right]^{12} - \left[\frac{\sigma_-}{R_{-i}} \right]^6 \right), \quad (10)$$

where $R_{-i} = |\mathbf{r}_0^i - \mathbf{x}_0^-|$ is the distance between the ion and the oxygen atom of the ith water molecule.

The energy associated with the partial collectivization of outer electron shells at contact distances between the ion and the molecule

$$U_{\text{c}}^{\text{I(–)–W}} = -U_0^- \sum_i (1 - s_-(R_{-i})). \quad (11)$$

The term that describes the saturation of bonds between the ion and molecules and also the unpaired effects of polarization interactions at small distances is as follows:

$$U_{\text{many body}}^{\text{W–I(–)–W}} = \alpha_0^- \left(\sum_{i<j} \left(\tilde{S}_-(R_{-i}) \tilde{S}_-(R_{-j}) \left(2\exp\left(-\frac{r_{\text{OH}}^{ij}}{b_0^-} \right) - 1 \right) \right)^{\tau_-} \right)^{\frac{1}{\tau_-}}, \quad (12)$$

where α_0^- and b_0^- are the amplitude and the characteristic radius of interaction and $r_{\text{OH}}^{ij} = \min(|\mathbf{r}_1^i - \mathbf{r}_0^j|, |\mathbf{r}_2^i - \mathbf{r}_0^j|, |\mathbf{r}_1^j - \mathbf{r}_0^i|, |\mathbf{r}_2^j - \mathbf{r}_0^i|)$ is the minimum distance between hydrogen of one molecule and oxygen of another one. The inclusion function has the form $\tilde{S}_-(R) = (1 - \tilde{s}_-(R))$ and $\tilde{s}_-(R)$ coincide with the accuracy up to exchange of R_L^- and R_U^- for the corre-

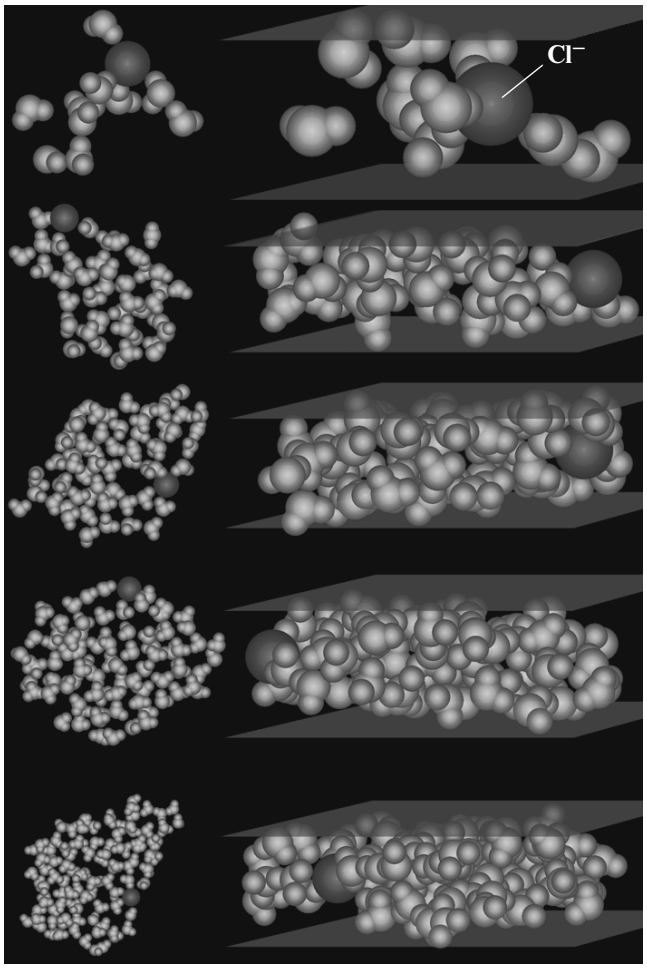

Fig. 1. A Cl^- ion fixed in the middle between the walls of a model planar pore 0.5 nm wide at 298 K, hydrated (from the top down) by 10, 40, 60, 80, and 100 water molecules. Left column: the view perpendicular to the pore plane; right column: the view along the pore plane.

sponding $\tilde{R}_L^-$ and $\tilde{R}_U^-$. The physical meaning of each term of the model can be found in [50].

For the Cl^- ion, based on the condition of the most accurate reproducibility of experimental free energy and entropy of the first six attachment reactions, the following parameters are found: $q_1^- = -1.06874\times10^{-19}$ C, $q_2^- = q_3^- = 0.53437\times10^{-19}$ C, $Q_0^- = 0.8072\times10^{-20}$ C, $Q_1^- = 1.52138\times10^{-19}$ C, $U_0^- = 2.28\times10^{-20}$ J, $R_L^- = 0.311$ nm, $R_U^- = 0.422$ nm, $\alpha_0^- = 0.225\times10^{-20}$ J, $b_0^- = 16$ nm, $\tau_- = 0.920$, $\tilde{R}_L^- = 0.422$ nm, $\tilde{R}_U^- = 0.68$ nm, $\alpha_w = 1.44\times10^{-3}$ nm, $\alpha_- = 3.59\times10^{-3}$ nm^3, $\varepsilon_0^- = 1.307\times10^{-21}$ J, $\sigma_- = 0.369$ nm. For the water–water interaction, the following standard values of SPC model parameters are taken: $\varepsilon_0^W = 1.08036\times10^{-21}$ J, $\sigma^W = 0.31656$ nm, $q_1 = -0.82e = -1.31372\times10^{-19}$ C, $q_2 = q_3 = 0.41e = 0.65686\times10^{-19}$ C. The position of charges q_1^-, q_2^-, q_3^- in the molecule coincides with the position of charges q_1, q_2, q_3.

3. RESULTS OF COMPUTER SIMULATION

Figure 1 exemplifies the current configuration of the chloride ion hydrate shell that grows in a planar pore from water vapors at room temperature. In the initial stage when the number of molecules in the hydrate shell does not exceed 10–20, the ion is located in the inner part of the cluster and the molecules form a system of chains radiating from the ion as from the center. The cluster shape resembles a starfish. The chains are polarized and in this stage the hydrate shell loose structure is associated with electrostatic repulsion between parallel dipole moments of chains. As the number of molecules in the shell increases, the chain structure transforms into a continuous net of interconnected water molecules in which individual chains are undistinguishable.

The analysis of the shape of atom-atom space correlation functions (are not shown here) demonstrated the high degree of stability of the hydrogen bond length between water molecules to the perturbations from the ion electric field. The positions of maximums of the oxygen-hydrogen correlation function of water molecules in the hydrate shell coincided within the hundredth fraction of nanometer with their positions in water under normal conditions. Substantial perturbations in the structure of hydrogen bonds in the ion field were observed in the orientational order, i.e., in the relative orientation of bonds between the neighboring pairs of molecules. The tendency towards the parallel orientation of neighboring hydrogen bonds was observed. No noticeable weakening or strengthening of this tendency was observed upon placing the ion into the nanopore.

In the first approximation, the effect of a narrow planar pore can be described as the reduction in the system dimensionality from three-dimensional (volume) to two-dimensional (planar). The competition between the loose chain structure and the compact form of the molecular cluster is the reflection of the competition between the energy and entropy components in system's free energy. As the hydrate shell size increases, the compact structures become more advantageous as reagrds energy. The decrease in the space dimension is associated with the relative decrease in the phase volume corresponding to "loose" molecular structures and the weakening of the entropy factor. Hence, as compared with hydration conditions in a bulk system, under the conditions of a planar nanopore, the compact structures gain a certain advantage over chain structures. The comparison with the results of simulations for free chloride ions in water vapors [52, 56, 57] shows that quantitatively this advantage turns out to be insufficient to exclude the

stage of chain formation; thus, as in the bulk systems, the evolution of the system under conditions of a planar nanopore includes the chain stage.

The next characteristic feature is the extrusion of the chloride ion from the central region of the cluster to its periphery. Figure 1 shows how after the transition from the chain structure to the compact form, the water molecules are gathered away from the ion. For this sort of binding between the ion and water molecules, it is more reasonable to speak not of the hydrate shell but of the surface adsorption of the ion by a cluster of water molecules.

The thermodynamic advantage of chloride-ion surface states during its interaction with clusters of water molecules was reliably reproduced under the conditions of hydration in bulk water vapors and confirmed by independent authors (see [52, 57] and references therein). The discussion concerned only the mechanism of this phenomenon. The data of [57] suggest that the decisive reason for the surface states of chloride ion in clusters of water molecules is the combination of two factors: the relatively high polarizability of the ion and the relatively high intrinsic dipole moment of a water molecule, which provides the high polarizability of the molecular cluster as a whole. The polarization energy depends on the electric field strength E by the quadratic law $(-\alpha\_E^2/2)$. The nonlinear dependence of the energy results in the fact that the simple addition of fields of individual molecules leads in the additional decrease in the ion polarization energy. In the configuration where all water molecules are located on one side of the ion all water molecules turn out to be oriented in the same manner with their dipole moments towards the ion so that their electric fields add up providing the lowest polarization energy of the ion and of the whole system.

In this configuration, the repulsion of parallel dipole moments of molecules is the counter-factor that increases the energy and destabilizes this state. The sufficiently high polarizability, as for the chloride ion, provides predomination of the first factor over the second and the stability of the ion surface states.

Thus, the stability of surface states is provided by their energy rather than by their entropic advantages. The entropy of a state is determined by the volume of available configuration space. This is why as the space dimension decreases, the energy effects strengthen as compared with entropy effects, all other factors the same. It should be expected that as we pass from bulk conditions to those of a planar nanopore, the effect of ion displacement to the surface of the cluster should not disappear but can even strengthen, being the energy effect.

The results of computer simulation confirmed these expectations. In the current configurations shown in Fig.1, the surface states of the ion stably prevail as soon as the number of molecules in the ion field becomes sufficient for the transition from the chain mode to the compact cluster. Thus, under conditions of planar pores, the effect of extrusion of the chloride ion from its own hydrate shell is as well pronounced as in bulk water vapors.

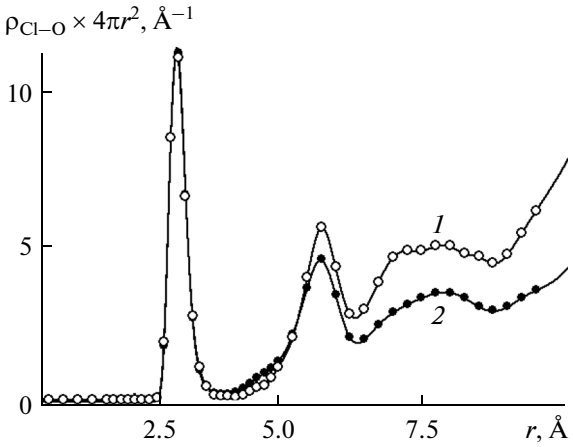

Fig. 2. Radial distributions: the average numbers of molecules per unit distance r from the Cl^- ion: (*1*) for the free ion in water vapors and (*2*) for the ion fixed in the middle between walls of a model planar pore 0.5 nm wide. Temperature 298 K, $\langle N \rangle = 39.5$.

In calculations by the method of bicanonical statistical analysis [58–67], the number of molecules in the system N is not fixed but fluctuates. The space correlation functions [30] chloride ion–oxygen atoms of water molecules $\rho_{Cl-O}(r)$ and chloride ion–hydrogen atoms of molecules $\rho_{Cl-H}(r)$ are normalized by the average number of molecules $\langle N \rangle$ in the system $\int_0^\infty \rho_{Cl-X}(r) 4\pi r^2 dr = \langle N \rangle$, X = O, H.

Figure 2 exemplifies the correlation function calculated under conditions of bulk vapor and in a planar nanopore. The comparison reveals the unexpectedly high stability of the correlation function towards the transition from the free ion to those in a nanopore. In both cases, the positions of the first three maximums that correspond to the first three hydrate layers coincide as well as their width. In a nanopore, the hydrate blob in the chloride ion field retains its pronounced layered structure with hydrate layers of the same thickness arranged at the same distances from the ion, like that observed for ion hydration under conditions free of steric limitations. It deserves mention that the pore width of 0.5 nm is smaller than the diameter of the first hydrate layer, so that the pore walls overlap all hydrate layers starting from the nearest to the ion. Moreover, as seen in Fig. 2, the perturbations in the layered structure of the bulb are reduced simply of discarding a part of molecules without any shift in the position of layers.

In the first approximation, the transition from conditions of bulk vapor to those of a planar nanopore corresponds to reducing the system dimensionality by unity. Whereas in the three-dimensional system the

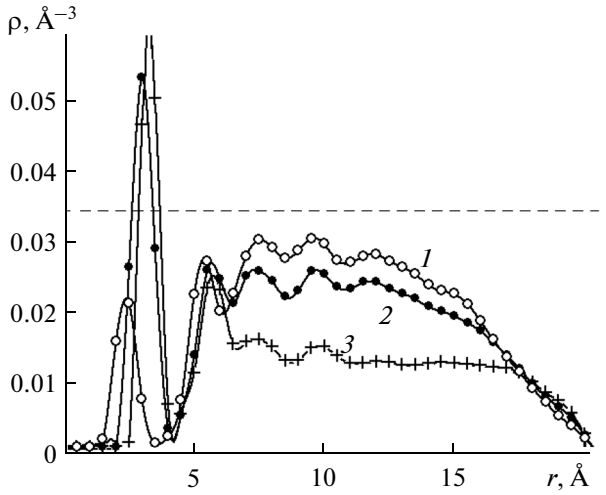

Fig. 3. Radial distributions of water molecules in parallel planes at distances, nm: (*1*), 0.025, (*2*) 0.125, and (*3*) 0.225 from the wall of a planar pore 0.5 nm wide in the field of a Cl^- ion fixed in the middle between walls. The distance *r* is counted from the line that passes through the ion center perpendicularly to the pore plane. Temperature 298 K, $\langle N \rangle = 99.5$. Dashed line is the water density at normal conditions.

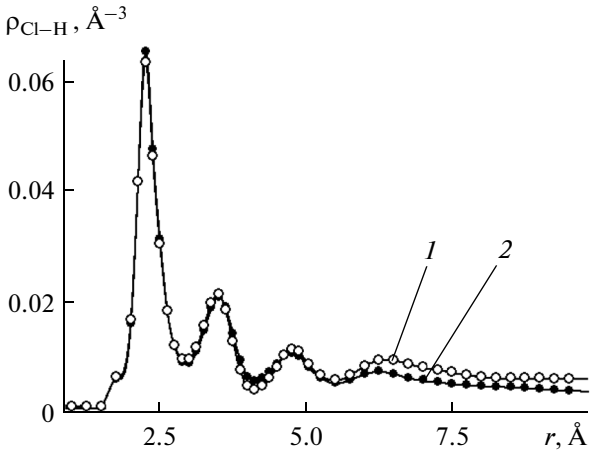

Fig. 4. Correlation function Cl^- ion–hydrogen atoms of water molecules for the same conditions and numeration as in Fig. 2.

configuration volume accessible for molecular motion increases with the distance as the third power of distance, in a planar system it decreases more slowly in proportion to the second power. Thus, the relative statistical weight of far distances decreases. This is why under conditions of a nanopore, a part of water molecules is redistributed from far to near distances, as evidenced by the lower values of the correlation function in the pore as compared with a free ion, at far distances from the ion (Fig. 2). A result of redistribution is the decrease in the average distance to the ion. This intrinsically geometrical effect caused by the decrease in the effective dimensionality of the system results in a small decrease in the energy of the system as a whole. The decrease in energy due to the decrease in the average distance to the ion in compensated to the considerable extent by the increase in energy due to destruction of a part of intermolecular bonds.

Figure 3 shows the radial distribution of molecules around the ion in the parallel sections at different distances from the pore wall. In the near-wall region, the majority of molecules are located far from the ion. However, this trend competes with the trend for compacting in the near-wall region. In pore's cross-section, on the averaged distribution, it is seen how the adsorbed material "leans" to pore walls leaving its central part depleted of molecules. The form of this distribution allows one to assume certain hydrophilicity of walls although this model did not presume the direct attraction to walls.

The effect of extrusion of molecules to walls is associated here with the orientation of dipole moments of molecules in the ion field and, as a consequence, with the repulsion of parallel dipoles. The repulsion forces operating between the molecules in the polarized bulb force out the molecules from the pore center to its walls. Thus, the effect of an ion inside a nanopore creates the effect of sticking of molecules to the walls. Obviously, this effect increases the hydrophilicity of walls.

The order in which the hydrogen atoms in molecules are arranged with respect to the ion is comparatively resistant to perturbations produced by pore walls. This follows from the coincidence of the position of maximums of the correlation function ion–hydrogen atoms of the molecule (Fig. 4) under conditions of hydration of a free ion and inside a pore. The first two maximums the nearest to the ion correspond to the distance from two hydrogen atoms of molecules in the first hydrate layer to the ion; the next two maximums correspond to the distance from the molecules of the second layer. The distances between the first and the second maximums and also between the third and the fourth maximums are close to the distance between hydrogen atoms in a molecule. The maximums far removed from one another and pertaining to one and the same pair point to the preferential orientation of molecules of the first two hydrate layers with the dipole moments strongly bent from the radial direction to the ion. In turn, this suggests that a substantial role in the interaction of a molecule with the ion field is played by its highest multifield moments and interactions mediated by the neighboring molecules.

The orientational order of molecules was analyzed in terms of angular distributions $W_\theta(\theta)$ and $W_\varphi(\varphi)$, where θ is the angle between the normal external with respect to the lower wall of the cavity and the vector of the intrinsic dipole moment of water molecule; φ is the rotation angle of the symmetry plane of molecule around its symmetry axis counted from the position

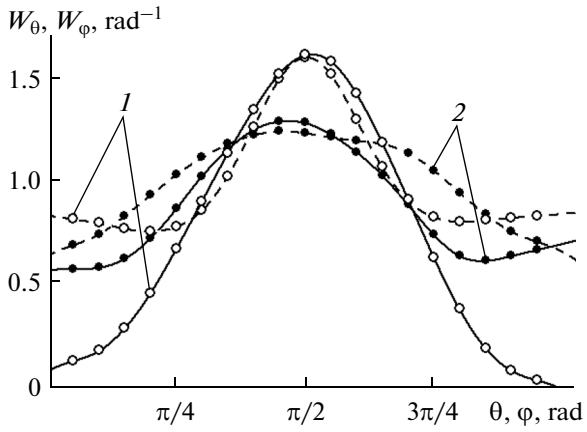

Fig. 5. Angular distributions of molecules in planes at distances, nm: (*1*) 0.025 and (*2*) 0.225 from the wall of a planar pore at the distance from the ion within 1 nm, under the same conditions as in Fig. 3. Solid line is the distribution over angle θ between the normal to the pore plane and the vector of the dipole moment of molecule; dashed line is the distribution over the rotation angle φ of the molecule around its symmetry axis.

where the molecular plane coincides with the plane in which the vectors of the normal to the wall and the dipole moment of the molecule lie (Fig. 5). The functions of distribution over angles are calculated in different layers located at different distances from the pore lower wall at the fixed distances z and are normalized as follows: $(1/2)\int_0^\pi W_\theta(\theta)\sin(\theta)d\theta = 1$ and $\int_0^\pi W_\varphi(\varphi)d\varphi = \pi$. For such normalization and in the absence of correlations, $W_\theta(\theta) = 1$ and $W_\varphi(\varphi) = 1$.

Distributions over the azimuth angle have a maximum at $\theta = \pi/2$. This means that the symmetry axes of molecules are oriented preferentially in parallel to the pore plane. The maximum at $\varphi = \pi/2$ of distributions over the rotation angle around the symmetry axis corresponds to the preferential orientation of the molecule plane in parallel to the pore plane. Thus, the presence of a pore affects first of all the molecular orientation. The effect strengthens in the immediate vicinity of walls and somewhat weakens in the internal part of the pore.

4. CONCLUSIONS

Hydration of ions is the initial stage of electrolyte formation in pores. The computer simulation allows the information on fundamental features of ion hydration in nanosized cavities to be obtained on the molecular level based on the fundamentally accurate statistical-mechanical approach.

The main results of this study are as follows.

As in bulk water vapors, the hydration of chloride ions in planar nanopores is accompanied by the displacement of the ion to the surface of the molecular cluster, which occurs after the shell reaches the size of 10–20 molecules. The displacement of the ion to the surface is the energy effect and does not weaken under the conditions of a nanopore.

The layered structure of the hydrate shell near the ion is resistant to perturbations from pore walls. The distances from the ion to the hydrate layers in the nanopore coincide with those in bulk water vapors with the accuracy higher than the hundredth part of nanometer.

The presence of the ion inside a nanopore creates the effect of sticking of molecules to the walls. The profile of molecular distribution in the pore cross-section demonstrates the increased volume density of molecules near the walls. The effect of molecules "creeping" to the walls may increase the effective hydrophilicity of walls in the presence of ion.

The orientational molecular order of the hydrate shell of the ion in a narrow planar pore is characterized by the preferential orientation of molecular planes in parallel to pore walls. The more monotonic orientational order in the pore as compared with the conditions in bulk water vapors determines, together with limitations in the translational motion of molecules, the lower entropy and the higher free energy of hydration. The effect of a narrow pore with nonhydrophilic walls as regards the free energy is entropic.

ACKNOWLEDGEMENTS

This study was carried out with the financial support by the Russian Foundation for Basic Research, projects nos. 12-03-90402-Ukr_a, 13-03-00062_a.

REFERENCES

1. Verbrugge, M.W. and Liu, P., *J. Electrochem. Soc.*, 2005, vol. 152, p. D79.
2. Chan, K. and Eikerling, M., *J. Electrochem. Soc.*, 2011, vol. 158, p. B18.
3. Robinson, D.B., Max Wu, C.-A., and Jacobs, B.W., *J. Electrochem. Soc.,* 2010, vol. 157, p. A912.
4. Frackowiak, E. and Beguin, F., *Carbon*, 2001, vol. 39, p. 937.
5. Gabelich, C.J., Tran, T.D., and Suffet, I.H., *Environ. Sci. Technol.*, 2002, vol. 36, p. 3010.
6. Ying, T.Y., Yang, K.L., Yiacoumi, S., and Tsouris, C., *J. Colloid Interface Sci.*, 2002, vol. 250, p. 18.
7. Yang, K.L., Yiacoumi, S., and Tsouris, C., *J. Electroanal. Chem.*, 2003, vol. 540, p. 159.
8. Hou, C.H., Liang, C.D., Yiacoumi, S., Dai, S., and Tsouris, C., *J. Colloid Interface Sci.*, 2006, vol. 302, p. 54.
9. Oldham, K.B., *J. Electroanal. Chem.*, 2008, vol. 613, p. 131.
10. Lozada-Cassou, M., Saavedra-Barrera, R., and Henderson, D., *J. Chem. Phys.,* 1982, vol. 77, p. 5150.
11. Lozada-Cassou, M., Olivares, W., and Sulbaran, B., *Phys. Rev. E*, 1996, vol. 53, p. 522.

12. Torrie, G.M. and Valleau, J.P., *Chem. Phys. Lett.*, 1979, vol. 65, p. 343.
13. Torrie, G.M. and Valleau, J.P., *J. Chem. Phys.*, 1980, vol. 73, p. 5807.
14. Torrie, G.M., Valleau, J.P., and Patey, G.N., *J. Chem. Phys.,* 1982, vol. 76, p. 4615.
15. Valleau, J.P. and Torrie, G.M., *J. Chem. Phys.*, 1982, vol. 76, p. 4623.
16. Torrie, G.M. and Valleau, J.P., *J. Phys. Chem.*, 1982, vol. 86, p. 3251.
17. Xu, D., Li, D., Leng, Y., and Chen, Y., *Mol. Simul.*, 2007, vol. 33, p. 959.
18. Lamperski, S. and Bhuiyan, L.B., *J. Electroanal. Chem.*, 2003, vol. 540, p. 79.
19. Boda, D., Fawcett, W.R., Henderson, D., and Sokolowski, S., *J. Chem. Phys.*, 2002, vol. 116, p. 7170.
20. Valisko, M., Henderson, D., and Boda, D., *J. Phys. Chem. B*, vol. 108, p. 16548.
21. Quesada-Perez, M., Martin-Molina, A., and Hidalgo-Alvarez, R., *J. Chem. Phys.*, 2004, vol. 121, p. 8618.
22. Taboada-Serrano, P., Yiacoumi, S., and Tsouris, C., *J. Chem. Phys.,* 2005, vol. 123, p. 054703.
23. Martin-Molina, A., Quesada-Perez, M., Galisteo-Gonzalez, F., and Hidalgo-Alvarez, R., *J. Phys.: Condens. Matter.*, 2003, vol. 15, p. 3475.
24. Quesada-Perez, M., Martin-Molina, A., and Hidalgo-Alvarez, R., *Langmuir,* 2005, vol. 21, p. 9231.
25. Martin-Molina, A., Quesada-Perez, M., and Hidalgo-Alvarez, R., *J. Phys. Chem. B*, vol. 110, p. 1326.
26. Malani, A., Ayappa, K.G., and Murad, S., *Chem. Phys. Lett.*, 2006, vol. 431, p. 88.
27. Hou, Ch.-H., Taboada-Serrano, P., Yiacoumi, S., and Tsouris, C., *J. Chem. Phys.*, 2008, vol. 128, p. 044705.
28. Tang, Y.W., Chan, K.Y., and Szalai, I., *J. Phys. Chem. B*, vol. 108, p. 18204.
29. Carrillo-Tripp, M., Saint-Martin, H., and Ortega-Blake, I., *Phys. Rev. Lett.,* 2004, vol. 93, p. 168104.
30. Khill, T., *Statisticheskaya mekhanika* (Statistical Mechanics), Moscow: Inostr. Lit., 1960.
31. Binder, K. and Kheerman, D.V., *Modelirovanie metodom Monte-Karlo v statisticheskoi fizike* (Modelling by the Monte Carlo Method in Statistical Physics), Moscow: Nauka. Fizmatlit, 1995.
32. Yashonath, S., *J. Chem. Phys.*, 2010, vol. 133, p. 114504.
33. Beladjine, S., Amrani, M., Zanoun, A., Belaidi, A., and Vergoten, G., *Comput. Theor. Chem.*, 2011, vol. 977, p. 97.
34. Varghese, A., Vemparala, S., and Rajesh, R., *J. Chem. Phys.*, 2011, vol. 135, p. 154902.
35. Li, W. and Mu, Yu., *J. Chem. Phys.*, 2011, vol. 135, p. 134502.
36. Longinotti, M.P., Carignano, M.A., Szleifer, I., and Corti, H.R., *J. Chem. Phys.*, 2011, vol. 134, p. 244510.
37. Reif, M.M. and Hunenberger, Ph.H., *J. Chem. Phys.*, 2011, vol. 134, p. 144104.
38. Murad, S., *J. Chem. Phys.*, 2011, vol. 134, p. 114504.
39. Molina, J.J., Lectez, S., Tazi, S., and Jean-Francois, M.S., *J. Chem. Phys.*, 2011, vol. 134, p. 014511.
40. Feng, H., Zhou, J., Lu, X., and Fichthorn, K.A., *J. Chem. Phys.,* 2010, vol. 133, p. 061103.
41. Sala, J., Guardia, E., and Marti, J., *J. Chem. Phys.*, 2010, vol. 132, p. 214505.
42. Rescic, J. and Linse, P., *J. Chem. Phys.*, 2008, vol. 129, p. 114505.
43. Dyer, P.J., Docherty, H., and Cummings, P.T., *J. Chem. Phys.*, 2008, vol. 129, p. 024508.
44. Duvail, M., Souaille, M., Spezia, R., and Cartailler, Th., *J. Chem. Phys.*, 2007, vol. 127, p. 034503.
45. Celebi, N., Angyan, J., Dehez, F., Millot, C., and Chipot, C., *J. Chem. Phys.*, 2000, vol. 112, p. 2709.
46. Dehez, F., Soetens, J.C., Chipot, C., Angyan, J., and Millot, C., *J. Phys. Chem. A*, 2000, vol. 104, p. 1293.
47. Dehez, F., Chipot, C., Millot, C., and Angyan, J.G., *Chem. Phys. Lett.*, 2001, vol. 338, p. 180.
48. Shevkunov, S.V., *Russ. J. Phys. Chem.*, 2004, vol. 78, p. 383.
49. Shevkunov, S.V., *Colloid J.*, 2004, vol. 66, p. 216.
50. Shevkunov, S.V., *Russ. J. Electrochem.*, 2013, vol. 49, p. 228.
51. Shevkunov, S.V., *Russ. J. Electrochem.*, 2013, vol. 49, p. 238.
52. Shevkunov, S.V., *Colloid J.*, 2009, vol. 71, p. 406.
53. Shevkunov, S.V., *Russ. J. Phys. Chem. A*, 2009, vol. 83, p. 972.
54. Jorgensen, W.L., Chandrasekhar, J., Madura, J.D., Impey, R.W., and Klein, M.L., *J. Chem. Phys.*, 1983, vol. 79, p. 926.
55. Stillinger, F.H. and Rahman, A., *J. Chem. Phys.*, 1974, vol. 60, p. 1545.
56. Shevkunov, S.V., *J. Adv. Chem. Phys.*, 2003, vol. 2, p. 109.
57. Shevkunov, S.V., *Russ. J. Phys. Chem. A*, 2011, vol. 85, p. 1584.
58. Shevkunov, S.V., *Khim. Fiz.*, 1983, no. 10, p. 1416.
59. Shevkunov, S.V., *Kolloidn. Zh.*, 1983, vol. 45, p. 1019.
60. Shevkunov, S.V., Martsinovskii, A.A., and Vorontsov-Vel'yaminov, P.N., *Teplofiz. Vys. Temp.*, 1988, vol. 26, p. 246.
61. Shevkunov, S.V., Martsinovski, A.A., and Vorontsov-Velyaminov, P.N., *Mol. Simul.*, 1990, vol. 5, p. 119.
62. Shevkunov, S.V., Lukyanov, S.I., Leyssale, J.-M., and Millot, Cl., *Chem. Phys.*, 2005, vol. 310, p. 97.
63. Shevkunov, S.V., *Colloid J.*, 2005, vol. 67, p. 509.
64. Lukyanov, S.I., Zidi, Z.S., and Shevkunov, S.V., *J. Mol. Struct.: THEOCHEM*, 2005, vol. 725, p. 191.
65. Lukyanov, S.I., Zidi, Z.S., and Shevkunov, S.V., *Chem. Phys.*, 2007, vol. 332, p. 188.
66. Lukyanov, S.I., Zidi, Z.S., and Shevkunov, S.V., *Fluid Phase Equilib.*, 2005, vol. 233, p. 34.
67. Shevkunov, S.V., *J. Exp. Theor. Phys.*, 2009, vol. 108, p. 447.

Translated by T. Safonova